Computational Materials Science 159 (2019) 1–11

Contents lists available at ScienceDirect

Computational Materials Science

journal homepage: www.elsevier.com/locate/commatsci

DFT study on CO oxidative coupling to DMO over Pd_4/TiO_2 and Pd_4/TiO_2-O_v: A role of oxygen vacancy on support

Yueting Cao[a], Lixia Ling[a,b,*], Hao Lin[a], Maohong Fan[c], Ping Liu[b], Riguang Zhang[d], Baojun Wang[d,*]

[a] College of Chemistry and Chemical Engineering, Taiyuan University of Technology, Taiyuan 030024, PR China
[b] State Key Laboratory of Coal Conversion, Institute of Coal Chemistry, Chinese Academy of Sciences, Taiyuan 030001, PR China
[c] Department of Chemical and Petroleum Engineering, University of Wyoming, 1000 E University Ave, Laramie, WY 82071, USA
[d] Key Laboratory of Coal Science and Technology of Ministry of Education and Shanxi Province, Taiyuan University of Technology, Taiyuan 030024, PR China

ARTICLE INFO

Keywords:
CO oxidative coupling to DMO
DFT
Pd_4/TiO_2
Oxygen vacancy

ABSTRACT

The reaction mechanisms for CO oxidative coupling to DMO on Pd_4 supported on TiO_2(0 0 1) catalysts were studied by using the density functional theory calculations with a Hubbard U correction (DFT + U). Two different supports including perfect TiO_2(0 0 1) and oxygen vacancy TiO_2(0 0 1) were investigated. The interaction between Pd_4 and supports showed that the binding energy of Pd_4 cluster with oxygen vacancy TiO_2(0 0 1) was stronger than that with the perfect TiO_2(0 0 1), and the relatively weak adsorption energy of CO was obtained on Pd_4/TiO_2-O_v, implied that it was easier for CO removing and reacting. In addition, reaction mechanisms of CO oxidative coupling to DMO on Pd_4/TiO_2 and Pd_4/TiO_2-O_v were studied, and the Pd_4/TiO_2-O_v catalyst showed higher activity than Pd_4-TiO_2. Moreover, compared with Pd(1 1 1), Pd_4/TiO_2-O_v not only reduced the amount of Pd, but also improved the activity of CO oxidative coupling to DMO. However, DMO and DMC were competitive products on Pd_4/TiO_2 and Pd_4/TiO_2-O_v, showed that they were with poor selectivity to DMO.

1. Introduction

As an important raw materials, dimethyl oxalate (DMO) is widely used in industrial production process. More importantly, the process of DMO hydrogenation to ethylene glycol has already successfully industrialized [1–3]. As we all known, DMO can be obtained from many processes, such as the esterification of oxalic acid with methanol [4] and the oxidative carbonylation of methanol. However, CO oxidative coupling to DMO has become the focus of people's attention due to its green and atom economy. Palladium-based heterogeneous catalysts with the pretty selectivity and reactivity for CO oxidative coupling which have been widely used to form the DMO [5]. However, the high price and large amount of Pd hindered its large-scale application in industry [6]. So it is the urgent problem that how to reduce the amount of Pd catalysts and keep the high catalytic performance. In order to decrease the amount of the noble catalysts, many attempts have been implemented, such as adding a second non-noble transition metals into Pd catalysts [7–9] and supporting the precious metals onto the carrier [10,11] to increase the dispersion of Pd catalysts and keep its activity at a high level.

Supported catalysts exhibit unusual catalytic properties and it is greatly impact on many heterogeneous catalytic reactions [12–16]. Compared to a pure Rh catalyst without a support, the Rh/TiO_2 catalyst exhibits better activity and selectivity of the ethanol formation [17]. The research of nitrobenzene hydrogenation over $Pd\text{-}B/SiO_2$ showed that the promoting effect of the SiO_2 support was mainly attributed to the stabilization of the Pd-B amorphous structure and the dispersion of the Pd active metal [18]. Moreover, Patel et al. [19] studied the hydrogenation of nitrobenzene using polymer anchored Pd(II) complexes, the results show that the catalyst showed high activity due to dispersion of more metal ions on the surface of the polymer. Meanwhile, a series of Pd-based loaded catalysts have been used in the reaction of CO oxidative coupling to DMO, such as Pd/Al_2O_3, Pd/MgO, Pd/AC, Pd/ZnO, Pd/TiO_2, they all show that the catalytic properties has been demonstrated to be strongly dependent on the support materials, and they all presented better activity and selectivity, and also reduced the amount of noble metals [20–24].

Previous studies showed that crystal defects have significant effect on the catalytic performance of catalysts [25–27]. For TiO_2 support, due to the defects and vacancy in the lattice, it shows better catalytic activity [28], and previous studies showed that anatase TiO_2 supported palladium catalyst performed strong metal-support interaction (SMSI)

* Corresponding authors at: No. 79 West Yingze Street, Taiyuan University of Technology, Taiyuan 030024, PR China.
E-mail addresses: linglixia@tyut.edu.cn (L. Ling), wangbaojun@tyut.edu.cn (B. Wang).

https://doi.org/10.1016/j.commatsci.2018.11.047
Received 15 June 2018; Received in revised form 16 November 2018; Accepted 26 November 2018

effect at low temperature, and presented high activity for the hydrogenation reaction of acetylene to ethylene [29]. Interestingly, studied the mechanisms of selective hydrogenation of acetylene on Pd_4 cluster, oxygen defective anatase (1 0 1) and rutile (1 1 0) titania supported Pd_4 cluster are studied recently, the result showed that anatase catalyst has higher selectivity of acetylene hydrogenation than rutile catalyst [30]. Moreover the type and the surface structure of the support markedly affect the catalytic property of the support catalysts and the active components. Previous researches showed that the oxygen vacancy plays a significant role in the enhancement of adsorption property and the catalytic property [31–35]. Recently, the adsorption of oxygen molecules on anatase (1 0 1) are studied, the results show the presence of oxygen vacancies greatly enhances the binding ability of oxygen molecules to the surface [36]. Meanwhile, previous research found that the oxygen vacancies increased the adsorption of Au clusters with CeO_2 surface sharply [37]. Thus, the oxygen vacancy TiO_2 is considered in this work, which removing one surface oxygen atom to present the oxygen vacancy surface.

Recently, owing to the high symmetry, high specific surface area, low surface atom coordination numbers, small metal Pd clusters have attracted more and more attention by researches [38,39]. As we all know, Pd_4 cluster, as the smallest magic cluster and three-dimensional cluster, are got widely concerned. Meanwhile, previous calculation results indicate that Pd_4 cluster similar adsorption properties with Pd_{13} cluster [33]. The previous studies also confirmed that the tetrahedral structure of Pd_4 cluster is more stable than that of planar one [40–42]. Therefore, the tetrahedral Pd_4 cluster has been selected in this work.

The (0 0 1) surface is considerably more reactive than the (1 0 1) one because of the higher surface energy [43]. Hence, in this work, aiming at illustrating the underlying mechanism and the influence of oxygen vacancy on the stability of catalyst, adsorption of reactants, reaction activity and selectivity, the reaction of CO oxidative coupling to DMO on perfect and oxygen vacancy anatase TiO_2(0 0 1) supported Pd_4 cluster have been systematically investigated using density functional theory (DFT) calculations. In a word, the results are expected to provide a good clue for designing an excellent catalyst with high activity and selectivity of CO oxidative coupling to DMO.

2. Computational models and methods

2.1. Calculation methods

A DFT + U calculations were performed in the Vienna ab initio simulation package (VASP) [44–47], the generalized gradient approximation (GGA) with the function of Perdew-Burke-Ernzerhof (PBE) was adopted to describe the exchange–correlation energies [48] and the electron-ion interactions were disposed by the projector-augmented wave (PAW) [44,47]. To analyze electron correlations in transition metal oxides, conventional DFT calculations based on the local density approximation was failed to predict the values of the band gap and band-gap states. Thus, DFT + U method [49] was introduced to evaluate the on-site coulomb interactions in the localized *d* orbital and exchange interactions, by adding an effective Hubbard-U parameter to express the repulsion between electrons on the same orbital [50]. In our calculations, the value of U parameter was determined to be 4 eV for the Ti atom [51,52]. The electronic wave functions were expanded in a plane wave basis with the kinetic cutoff energy of 400 eV [53], and a Gaussian smearing parameter of SIGMA = 0.2 eV was used to improve convergence of states near the Fermi level. A Monkhorst-Pack *k*-points grid of 6 × 6 × 6 was carried out to sample the bulk of TiO_2. The *k*-point of 2 × 2 × 1 and 3 × 3 × 1 were selected to calculate adsorption energies of CO and OCH_3 on Pd_4/TiO_2, which are −284.1 and −283.6 kJ·mol^{-1} for CO adsorption, −227.9 and −228.0 kJ·mol^{-1} for the adsorption of OCH_3. It is implying that there is little influence on the adsorption energy with different *k*-point. Therefore, considering the efficiency of calculation, the *k*-point of 2 × 2 × 1 was thought to be feasible and enough for this calculated system. A force difference between two steps of less than 0.03 eV Å^{-1} was used as the criterion for convergence of ionic relaxation. The relaxation of the electronic degrees of freedom is assumed to be converged, if the total energy change and the band structure energy change between two steps are both smaller than 1 × 10^{-5} eV. The vacancy formation energy of TiO_2(0 0 1) and the binding energy E_b between Pd_4 and TiO_2 are calculated by the following formulas:

$$E_{f(O)} = E_{def} - E_{per} + 1/2E_{O_2} \quad (1)$$

and

$$E_b = E_{Pd_4} + E_{TiO_2} - E_{Pd_4/TiO_2} \quad (2)$$

where E_{def}, E_{per}, and E_{O2} are energies of the defect system, the perfect system and the free molecular oxygen. $E_{Pd4/TiO2}$, E_{Pd4} and E_{TiO2} are the energy of Pd_4 located on the TiO_2, the energy of isolated Pd_4 and the energy of isolated TiO_2.

The adsorption energy, E_{ads} and the activation energy E_a are defined by using the following equations:

$$E_{ads} = E_{tatal} - E_{Pd_4/TiO_2} - E_{adsorbates} \quad (3)$$

and

$$E_a = E_{TS} - E_{IS} \quad (4)$$

where E_{total} and $E_{adsorbates}$ were total energies of total adsorbed systems and isolated adsorbates. E_{TS}, and E_{IS} represent the energies of the TS (transition state), and IS (initial state), respectively.

Reaction pathways have been investigated using the climbing-image nudged elastic band method (CI-NEB) [54,55], and the image close to the transition structure can be found. Furthermore, the dimer method is used to optimize the image and obtain the transition state [56,57]. In this study, the optimized transition state structure was deemed to be converged when the forces for all atoms was less than 0.05 eV/Å, and there is only one harmonic vibrational frequency in every transition state structure.

2.2. Calculation models

The symmetric periodic slab models were used for anatase structure, the calculated lattice constant of bulk TiO_2(0 0 1) structure (a = 3.84 Å, c = 9.63 Å, c/a = 2.5) is greatly agreement with the experimental value [58]. On the TiO_2(0 0 1) surface, there are two types of O atoms, which are O_1 and O_2, and the vacancy formation energies are 195.1 and 354. 7 kJ·mol^{-1}. It can be seen that the formation of vacancy by removing O_2 is more difficult than O_1. However, the binding energies between Pd_4 cluster and TiO_2 with O_1 vacancy and O_2 vacancy are 354.4 and 407.6 kJ·mol^{-1}, respectively. It indicates that there is a stronger binding ability between Pd_4 cluster and TiO_2 with the oxygen vacancy of O_2. In addition, the activity energy barrier of CO + OCH_3-$COOCH_3$ on the Pd_4 cluster supported on TiO_2 with vacancy of O_1 and O_2 are 118.5 and 74.9 kJ·mol^{-1}, which means that Pd_4 supported on TiO_2 with O_2 may show higher catalytic performance. As a result, combining with the binding energy of Pd_4 and oxygen vacancy surface, as well as the activity energy barrier of first step, TiO_2 with the oxygen vacancy of O_2 was chosen. In addition, the size of supercell was investigated. The oxygen vacancy formation energies on TiO_2(0 0 1) with 2 × 2, 3 × 3, and 4 × 4 supercell was studied, and there is little effect of supercell size on the formation of oxygen vacancy. Meanwhile, adsorption energies of important intermediate $COOCH_3$ on three Pd_4/TiO_2-O_v with 2 × 2, 3 × 3, and 4 × 4 supercell were studied, and there is little difference between three adsorption energies, as shown in Fig. 1. In addition, 3 × 3 supercell was widely used in previous work [59–61]. Therefore, we chose 3 × 3 supercell in this research. Both perfect and oxygen vacancy TiO_2(0 0 1) slabs were with the thickness of four O—Ti—O repeat units including 12 atomic layers. The bottom six atomic layers were fixed in all structural optimizations, as shown in

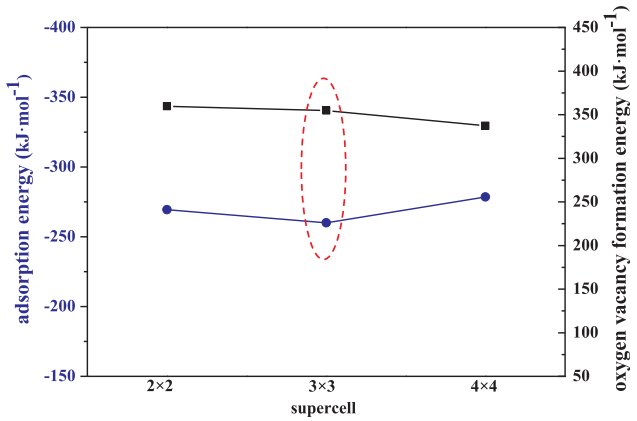

Fig. 1. The oxygen vacancy formation energies of TiO_2(0 0 1) with 2 × 2, 3 × 3, and 4 × 4 supercell and adsorption energies on three Pd_4/TiO_2-O_v catalysts.

Fig. 2. A vacuum of 15 Å was used for all slab. The isolated molecules and radicals were optimized in a large cell of 10 × 10 × 10 Å. We have considered the influence of adsorption and reaction when a dipole correction was added to system. The results showed that the co-adsorption energy of CO and OCH_3 was 442.9 kJ·mol^{-1} with a dipole correction, it is similar with that energy (−441.2 kJ·mol^{-1}) without dipole correction. The adsorption energies of $COOCH_3$ are 260.9 and 259.9 kJ·mol^{-1} with and without dipole correction. Meanwhile, the result of the first elementary step (CO + OCH_3 → $COOCH_3$) showed that the difference of energy barrier and reaction energy between these two cases are 4.9 and 0.7 kJ·mol^{-1}. That all implied that little difference exists when the dipole correction is added into system. The adsorption energies for molecule such as CO on surface are with little difference with and without dipole correction in previous study [62]. Thus, dipole correction is neglected and the former research has the same treatment method [63]. In fact, it was handled with neutral oxygen vacancy in this work, and previous studies on oxygen vacancies were also treated as neutral oxygen vacancies [64,65].

Several possible active sites for Pd_4 cluster on both perfect and oxygen vacancy TiO_2(0 0 1) surface were first considered, relaxed structures and their adsorption energies are shown in Figs. 3 and 4. The most stable structure of Pd_4/TiO_2 (a) is with the energy of 360.1 kJ·mol^{-1} and the most stable structure of Pd_4/TiO_2-O_v (c′) is with the energy of 407.6 kJ·mol^{-1}. And the possible adsorption sites of Pd_4/TiO_2 and Pd_4/TiO_2-O_v are marked in Fig. 5, it includes top (T), bridge (B1, B2, B3, B4) and 3-fold hollow (Hcp) sites.

3. Results and discussion

3.1. The structure properties of Pd_4/TiO_2 and Pd_4/TiO_2-O_v

The interactions between Pd_4 cluster and two different TiO_2(0 0 1) surfaces are discussed. Firstly, bond lengths between Pd-Pd in these two catalysts are considered, the average bond length is 2.652 Å for Pd_4/TiO_2 catalyst, while the value is elongated in Pd_4/TiO_2-O_v of 2.692 Å. The bond lengths of Pd-Ti were also taking into account, and the data are displayed in Table 1. The shorter the bond length of Pd-Ti, the stronger the ability of Pd combine with the carrier. We can see that the stability of Pd_4/TiO_2-O_v is stronger than that of Pd_4/TiO_2. Secondly, the binding energy E_b of Pd_4 cluster with perfect and oxygen vacancy TiO_2(0 0 1) surfaces are 360.1 and 407.6 kJ·mol^{-1}, the more positive the value is, the interaction between active component and support is the stronger, which indicates that oxygen vacancy surface shows stronger binding ability with Pd_4 clusters. It is consistent with former studies, small Pd_n(n = 1–4) clusters have the larger adsorptive energies with oxygen vacancy TiO_2 than with perfect TiO_2, more importantly, it also proved that Pd_4 and Pd_5 clusters with 3D structures are more stable on TiO_2 [66]. Moreover, the binding energies between metals with both perfect and oxygen vacancy MgO(1 0 0) have also shown that stronger interaction between metal and oxygen vacancy MgO(1 0 0), in which binding energies of 79.5, 105.4, 195.4 and 72.4 kJ·mol^{-1} for metals (metal = Ni, Pd, Pt or Cu) on perfect MgO surface and 107.9, 249.8, 356.5 and 79.9 kJ·mol^{-1} on the MgO-O_v surface, the results also confirmed that the oxygen vacancy surface exhibits excellent binding ability with metals compare to the perfect surface [67].

In addition, in order to investigate the influence of oxygen vacancy, the projected density of states (*p*DOS) and *d*-band center of Pd_4 cluster

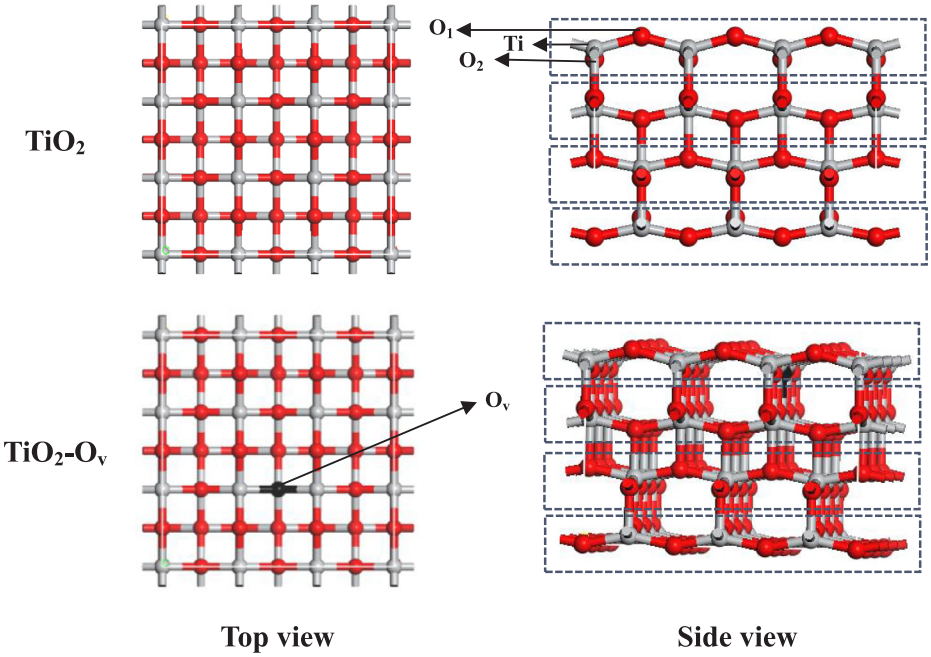

Fig. 2. Top and side views of the optimized structures of perfect and oxygen vacancy TiO_2(0 0 1) models. Red, silvery spheres represent O, Ti atoms, and black sphere represents oxygen vacancy.

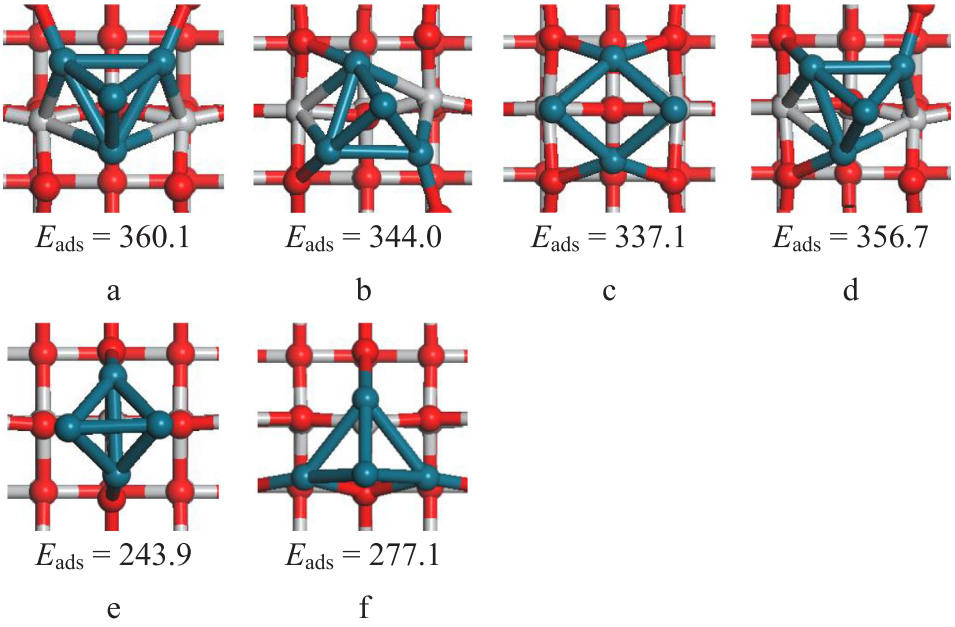

Fig. 3. The possible structures of Pd_4/TiO_2 model. Red, silvery, blue spheres represent O, Ti, Pd atoms, respectively.

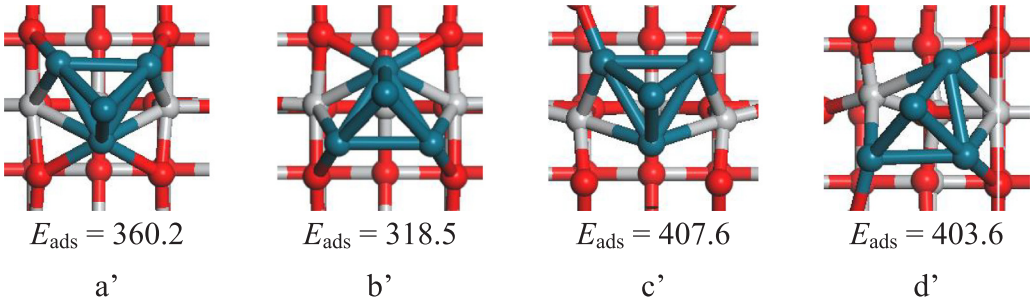

Fig. 4. The possible structures of Pd_4/TiO_2-O_v model. Red, silvery, blue spheres represent O, Ti, Pd atoms, respectively.

on TiO_2 and TiO_2-O_v are analyzed. It is known that different catalysts exhibit different *d*-band centers, especially the presence of O vacancies, which change the *d*-band. The electronic structure of the metal catalyst surface has a deep relationship with the adsorption properties and catalytic property. To some extent, *d*-band center exhibits the energy level of the metal's *d*-orbitals, and as a vital parameter to determine the ability of the surface to bond with adsorbates, and to predict the adsorption ability and catalytic activity of catalysts [68]. In this work, the projected density of states (*p*DOS) and *d*-band center of Pd_4 cluster on TiO_2 and TiO_2-O_v are analyzed. The *d*-band center is calculated by the following equation the *d*-band center is calculated by the following equation [69]:

$$\varepsilon_d = \frac{\int_{-\infty}^{+\infty} E\rho_d(E)dE}{\int_{-\infty}^{+\infty} \rho_d(E)dE} \quad (5)$$

where ρ_d represents the density of states projected onto Pd atom's *d*-band, and *E* is the energy with respect to the Fermi energy, and the integral limits are $-\infty \sim +\infty$.

The *d*-band centers of Pd_4/TiO_2 and Pd_4/TiO_2-O_v are −1.69 and −1.82 eV (Fig. 6), obviously, the *d*-band center of Pd_4/TiO_2-O_v is far away from the Fermi energy. CO as an important reactant in CO oxidative coupling to DMO is necessary to study its adsorption firstly. As listed in Table 1, the adsorption energies of CO are −159.6 to −284.1 kJ·mol^{-1} and −144.8 to −193.3 on Pd_4/TiO_2 and Pd_4/TiO_2-O_v, respectively. Obviously, Pd_4/TiO_2-O_v catalyst exhibits relatively low adsorption ability. In order to reveal the microscopic reason of CO adsorption, the *d*-band center, as a key parameter, is usually selected to measure the distribution of solid energy levels, and it can also reveal the ability to eject an electron to the adsorbed molecule from metal *d*-band. More importantly, previous studies showed that the atomic C adsorption strength on Ni(1 0 0), Ni(5 5 3), and Ni(1 1 1) decreased for methane dissociation reaction on Ni catalysts, which originates from the reduction of the *d*-band center of the surface Ni atoms [70]. Moreover, some researchers also proved that there is a deep relationship between the *d*-band center and the catalytic activity [65,71]. The binding ability between the palladium surface and adsorbates is not too weak and not too strong, which shows a high catalytic activity [72]. In this work, weak adsorption capacity of CO on Pd_4/TiO_2-O_v indicates that adsorbates are easy to remove on catalyst, and then they are easier to react with each one, thus shows high activity. Therefore, the activity of these two catalysts are investigated in the following sections via the reaction mechanism.

3.2. CO oxidative coupling to DMO on perfect and oxygen vacancy TiO_2 support Pd_4 catalysts

3.2.1. The reaction mechanism of CO oxidative coupling to DMO

In order to probe into the effect of support on the formation of DMO, it is necessary to understand the possible reaction pathway of the DMO formation. For the reaction of CO oxidative coupling to DMO, previous research showed that the fracture energy barrier of O-N in CH_3ONO (MN) leading to CH_3O and NO is 0.03 eV on the Pd based catalysts, which indicates that MN is easy to dissociate [73]. Therefore, the dissociation of MN is ignored. Two feasible paths have been obtained in

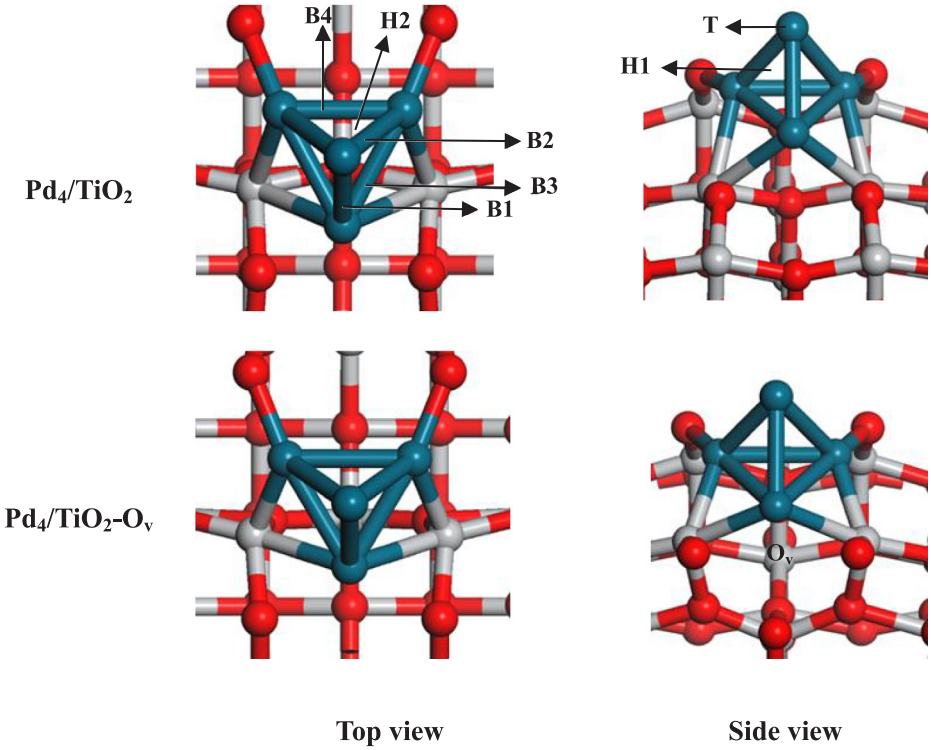

Fig. 5. The optimized structures of top and side views of Pd_4/TiO_2 and Pd_4/TiO_2-O_v model. Red, silvery, blue spheres represent O, Ti, Pd atoms, respectively.

Table 1
The average atomic distance ($d_{Pd\text{-}Ti}$ and $d_{Pd\text{-}Pd}$) and CO adsorption energies E_{ads}(CO) for Pd_4/TiO_2 and Pd_4/TiO_2-O_v catalysts.

Parameters	Pd_4/TiO_2	Pd_4/TiO_2-O_v
Pd-Ti distance (Å)	2.686	2.436
Pd-Pd distance (Å)	2.652	2.692
E_b (kJ·mol^{-1})	−360.1	−407.6
E_{ads}(CO) (kJ·mol^{-1})	−159.6 to −284.1	−144.8 to −193.3

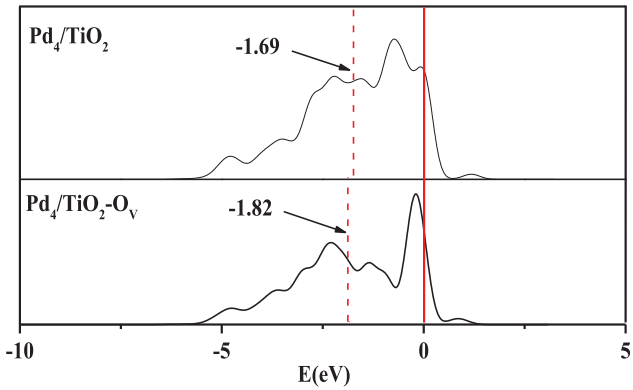

Fig. 6. Projected density of states (*p*DOS) plots of the *d*-orbitals for the Pd atoms of Pd_4/TiO_2 and Pd_4/TiO_2-O_v catalysts. The red vertical dashed line represents the location of *d*-band center, and the red vertical solid line indicates Fermi energy level.

this work, as shown below:

Path 1: $CO + OCH_3 \rightarrow CO + OCH_3$ $(COOCH_3) \rightarrow COOCH_3$ $(COOCH_3) \rightarrow$ DMO

Path 2: $CO + OCH_3 \rightarrow COOCH_3 + CO \rightarrow OCCOOCH_3 + OCH_3 \rightarrow$ DMO

3.2.2. CO oxidative coupling on Pd_4/TiO_2

All of the possible co-adsorbed conformations of CO and OCH_3 were investigated for the first step on Pd_4/TiO_2 catalyst. The co-adsorption of CO and OCH_3 are on two facets of Pd_4/TiO_2 when CO and OCH_3 are placed at H1-H1, T-B1, T-B3, B1-B3 and B2-B2 sites in original structures, as shown in Fig. 7. They are almost no chance to react with each other to form $COOCH_3$ intermediate. Five possible co-adsorption configurations are obtained for the reaction of CO and OCH_3, one of which is that CO and CH_3O adsorb on B2 and B(Pd-Ti) sites (h), other four structures (b, f, i and j) are that CO is at H1 site and OCH_3 is at T site. These two types of co-adsorption configurations are considered as reactants, and the formation of $COOCH_3$ is investigated, the energy barrier and reaction energy are shown in Table 2. We can found that the formation of $COOCH_3$ is easier when CO and CH_3O are at B2 and B(Pd-Ti) sites with an energy barrier of 95.1 kJ·mol^{-1}, which proceeds to the next step.

In Path 1, when the first $COOCH_3$ is formed via TS1, another $COOCH_3$ is formed through TS2 with an energy barrier of 36.9 kJ·mol^{-1} (Fig. 8). Finally, DMO is formed by two $COOCH_3$ coupling via TS3 and this step needs to overcome a higher energy barrier of 146.4 kJ·mol^{-1}, which is the rate determining step in Path 1. The same rate determining step has been obtained on the Pd(1 1 1) surface in our precious work [74]. However, it is only 120.6 kJ·mol^{-1} for this step, which is lower than that on the Pd_4/TiO_2 catalyst. For Path 2, the first step is the same as the Path 1, and then CO attacks $COOCH_3$ to generate a new C-C bond via TS4, which is a process from C1 to C2 and the energy barrier is 173.5 kJ·mol^{-1}. At last, $OCCOOCH_3$ intermediate combines with OCH_3 to produce the target product DMO via TS5, this elementary reaction needs to overcome an energy barrier of 93.6 kJ·mol^{-1}. The formed DMO is similar that in Path 1, both of two DMO absorb on the top site. Obviously, the step of CO reacting with $COOCH_3$ is the rate determining step with the highest elementary energy barrier of 173.5 kJ·mol^{-1} in Path 2, which is extremely difficult to occur. It can be found that Path 1 is more favorable than Path 2 on the perfect TiO_2 support Pd_4 catalyst as the lower energy barrier for rate determining step of 146.4 kJ·mol^{-1}. Similarly, $COOCH_3$-$COOCH_3$ coupling route (Path 1) is the favorable

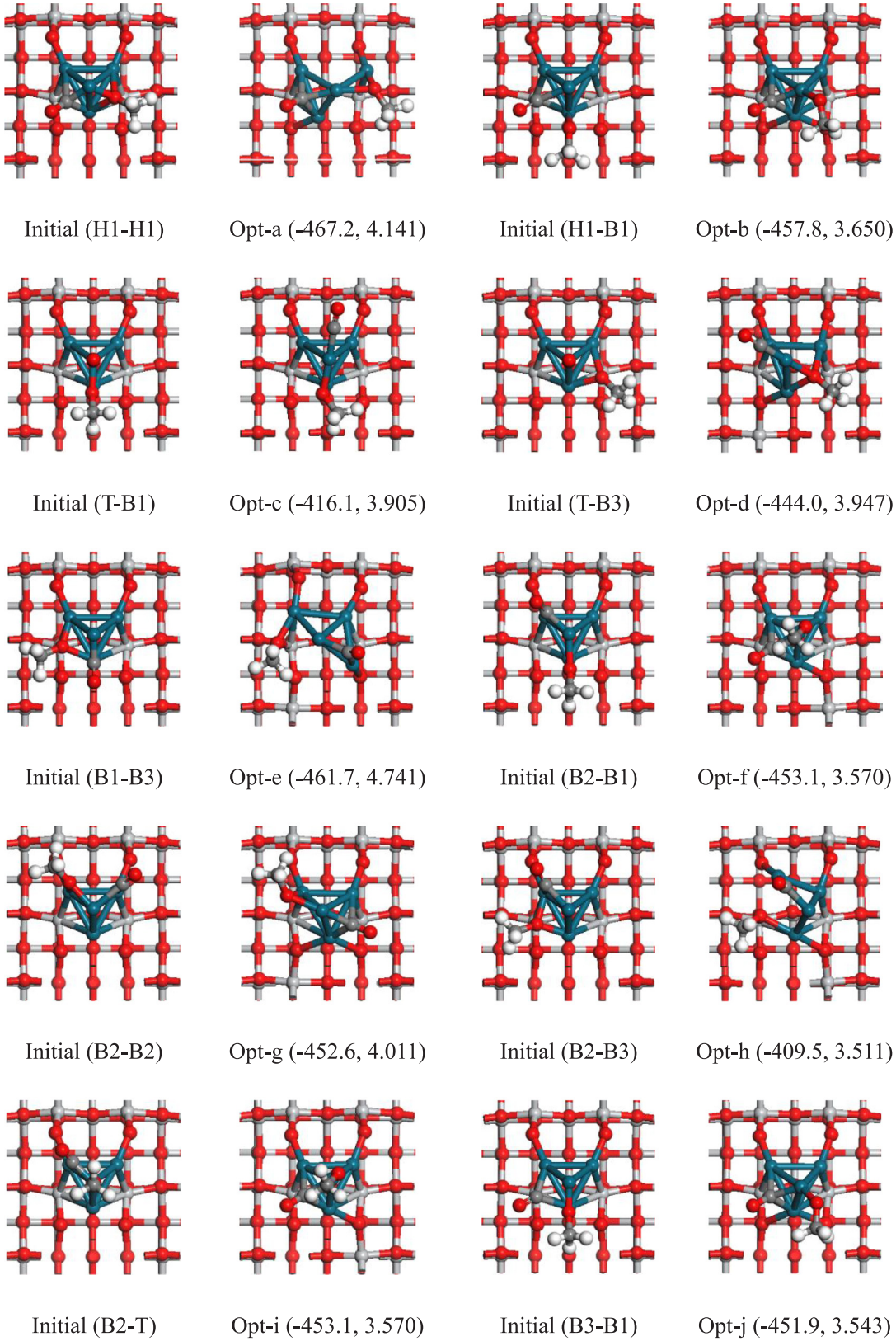

Fig. 7. The initial and optimized co-adsorption configurations of CO and OCH_3 on Pd_4/TiO_2 catalyst with the corresponding co-adsorption energies ($kJ{\cdot}mol^{-1}$) and the distance of C−O (Å). Red, silvery, blue, grey and white spheres represent O, Ti, Pd, C and H atoms, respectively.

path on Pd(1 1 1), Pd-Al(1 1 1) [74], Pd_{13}, $Al@Pd_{12}$, $Ag@Pd_{12}$ [75], Pd/SVG and Pd_4/SVG catalysts [76].

3.2.3. DMO formation on Pd_4/TiO_2-O_v

Two reaction processes of CO oxidative coupling to DMO on Pd_4/TiO_2-O_v are shown in Fig. 9. For the formation of $COOCH_3$, the energy barrier is 74.9 $kJ{\cdot}mol^{-1}$ which is smaller than that on the Pd_4/TiO_2

Table 2
The energy barrier (E_a) and reaction energy (E_r) of first elementary step for CO oxidative coupling to DMO on Pd_4/TiO_2 catalyst.

Elementary reaction	E_a (kJ·mol^{-1})	E_r (kJ·mol^{-1})
CO + OCH_3 (h) → $COOCH_3$ (H1)	95.1	3.0
CO + OCH_3 (j) → $COOCH_3$(H1)	195.6	45.4

catalyst, it means that $COOCH_3$ is easier to form on Pd_4/TiO_2-O_v catalyst. This may be due to the strong electron interaction between the oxygen vacancy and the Pd_4 cluster, which results in the weak adsorption of CO on the catalyst surface, therefore, CO move easily and react with OCH_3. In Path 1, following the completion of first catalytic reaction for first $COOCH_3$ formation, another CO and OCH_3 on the adjacent T-site and B-site react with each other leading to the formation of another $COOCH_3$ by TS2′, which needs an energy barrier of 77.0 kJ·mol^{-1} with an exothermic energy of 10.9 kJ·mol^{-1}. Subsequently, two stable intermediates $COOCH_3$ coupled to form DMO via TS3′ and overcoming an energy barrier of 66.7 kJ·mol^{-1}, which is lower than that on Pd_4/TiO_2 with 146.4 kJ·mol^{-1}. In this path, the formation of the second $COOCH_3$ is the rate determining step, which is different from that on Pd_4/TiO_2. For the other path for the formation of DMO, the C—C coupling occurs via CO attacking $COOCH_3$ by TS4′, it overcomes a larger energy barrier of 155.2 kJ·mol^{-1} leading to a stable intermediate $OCCOOCH_3$. Finally, OCH_3 attacks $OCCOOCH_3$ via TS5′ to DMO with the energy barrier and reaction energy of 48.7 and −80.1 kJ·mol^{-1}. In this path, the generation of new C—C bond is the rate determining step. It can be seen that Path 1 is the favorable route for CO oxidative coupling to DMO. In addition, Pd_4/TiO_2-O_v shows higher activity than Pd_4/TiO_2 comparing with activation energies on two catalysts, which is even higher than that of the Pd(1 1 1) surface (77.0 *vs* 118.4 kJ·mol^{-1}) [77]. Moreover, according to latest research by our work [74], the rate

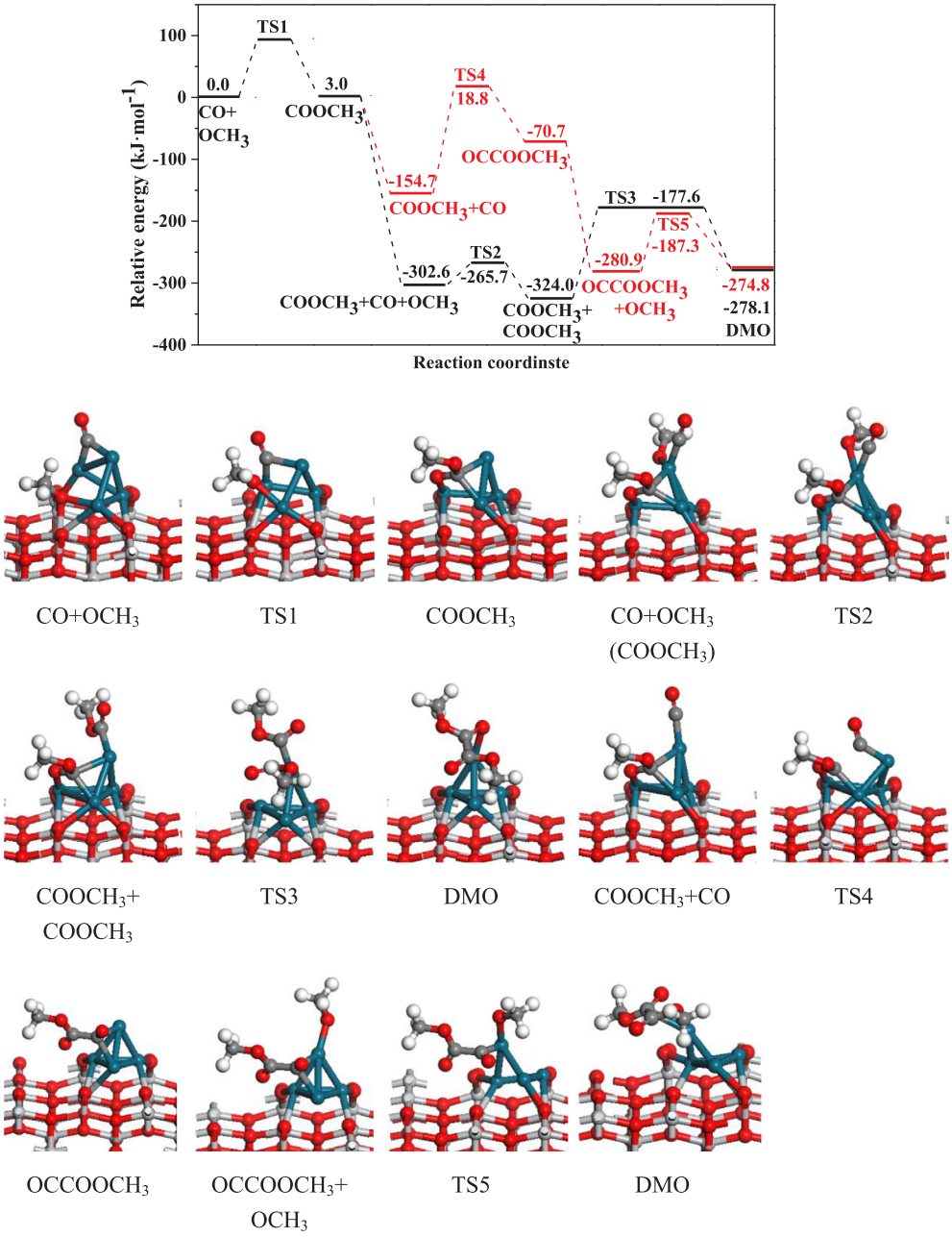

Fig. 8. The potential energy profile for the most favorable formation pathway of CO oxidative coupling to DMO on Pd_4/TiO_2 catalyst together with the structure of Product, Reactant and Transition State. Red, silvery, blue, grey and white spheres represent O, Ti, Pd, C and H atoms, respectively.

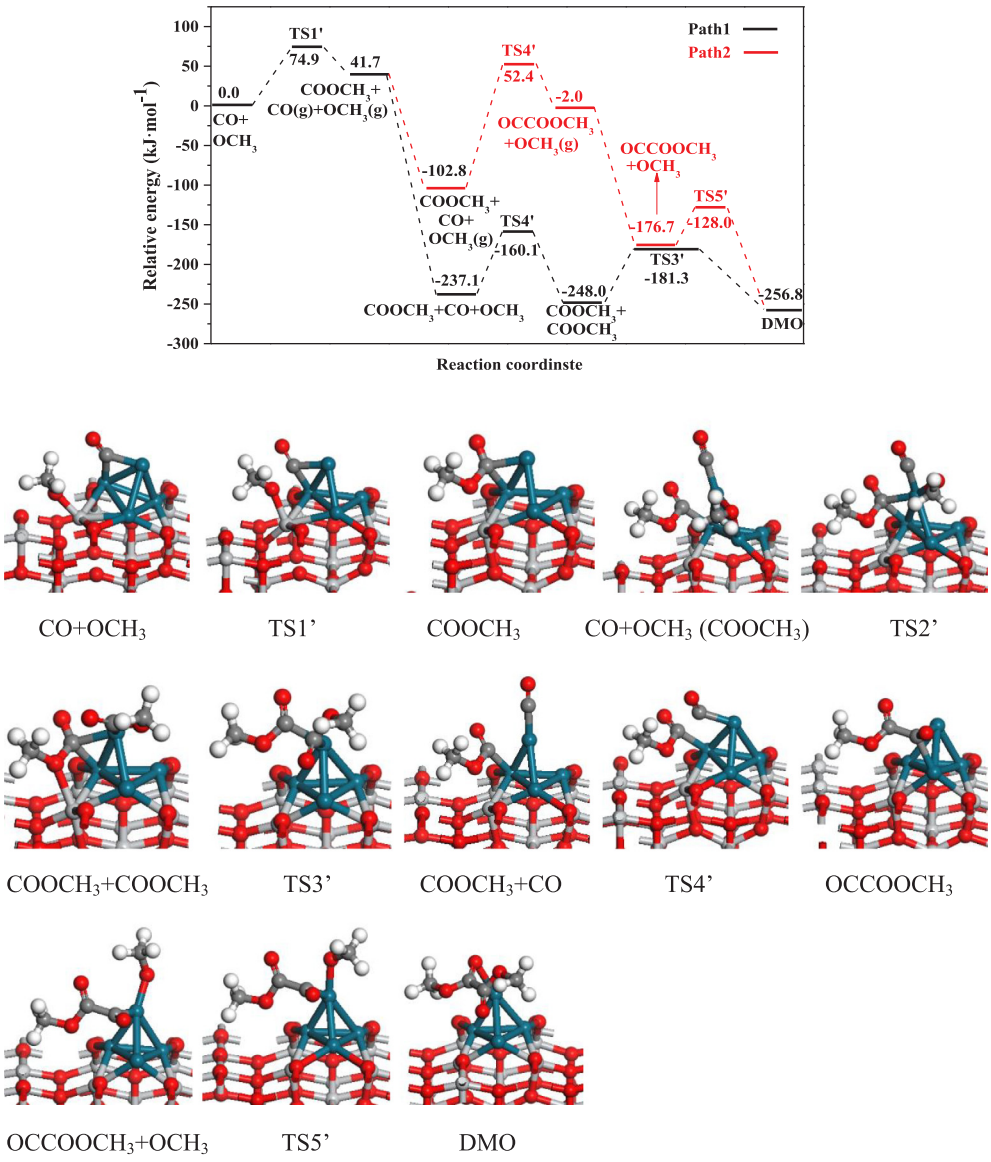

Fig. 9. The potential energy profile for the most favorable formation pathway of CO oxidative coupling to DMO on Pd_4/TiO_2-O_v catalyst together with the structure of Product, Reactant and Transition State. Red, silvery, blue, grey and white spheres represent O, Ti, Pd, C and H atoms, respectively.

determining step energy is 113.0 kJ·mol^{-1} on Pd-Al(1 1 1) catalyst, means that Pd_4/TiO_2-O_v catalyst also exhibits better catalytic activity than Pd-Al bimetallic catalyst.

3.2.4. Selectivity of catalysts to DMO

It is said that selectivity is an important parameter to measure the catalysts besides the catalytic activity. For CO oxidative coupling reaction, Dimethyl carbonate (DMC) is the main by-product. Therefore, the selectivity of DMO is also considered in this work, and the results were shown in Figs. 10 and 11.

DMC is formed by OCH_3 attacked $COOCH_3$, which has already detected by calculation and experiment [77–79]. On Pd_4/TiO_2, a high energy barrier of 150.4 kJ·mol^{-1} needs to be overcome to form DMC, which is slightly higher than the activity barrier of forming DMO in Path 1 (146.4 kJ·mol^{-1}), the difference between the formation of DMO and DMC is 4.0 kJ·mol^{-1}. It means that the formation of DMO and DMC are competitive reaction on Pd_4/TiO_2, which shows that Pd_4/TiO_2 catalyst exhibits low selectivity towards DMO. Then, we consider the selectivity of Pd_4/TiO_2-O_v.

In Fig. 11, the formation of DMC needs to overcome a slightly lower energy barrier (63.0 kJ·mol^{-1}) via TS6′, compared with the active energy barrier (77.0 kJ·mol^{-1}) of forming the second $COOCH_3$ by CO and OCH_3 in Path 1. The difference between the formation of DMO and DMC is 14.0 kJ·mol^{-1}, which indicates that the selectivity of DMO on Pd_4/TiO_2-O_v is poor.

3.2.5. The role of oxygen vacancy on support in activity and selectivity

Oxygen vacancy on the surface of anatase TiO_2 has obviously influence on the stability of catalyst, adsorption of reactants, reaction activity and selectivity. The stability of catalyst is enhanced when the oxygen vacancy appears on the TiO_2 surface. The adsorption energy becomes smaller when oxygen vacancy exists for the adsorption of reactants, which is consistent with the results about the co-adsorption of C_xH_y and H on Pd_4/TiO_2-O_v catalysts [33] and the adsorptions of CH_x on the perfect and oxygen vacancy MgO(0 0 1) supported Ni_4 catalysts [80]. The existence of oxygen vacancy enhanced the catalytic activity between Pd_4 cluster and TiO_2-O_v comparing with the perfect TiO_2 support, the similar result has been obtained that a single Pd atom loaded on an oxygen vacancy site of the MgO(1 0 0) surface is more beneficial for the cyclization reaction of acetylene to benzene than perfect surface [81]. Meanwhile, for the effect of oxygen vacancy on the selectivity, M-TiO_2-O_V (M = Ag, Pt, and Pd) nanocomposites can be

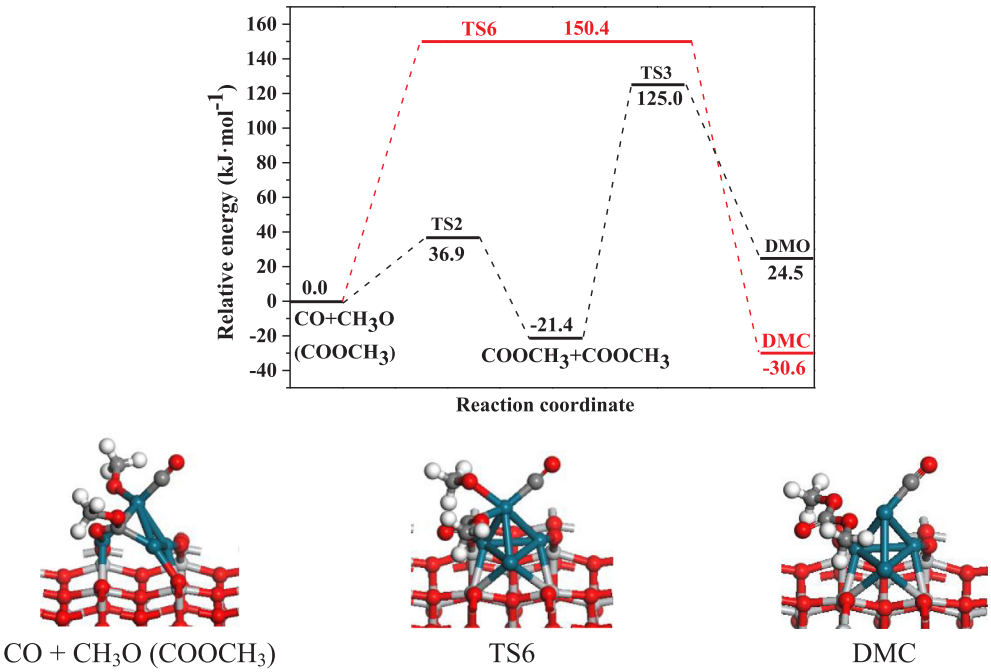

Fig. 10. The comparison of the simplified potential energy profile for the pathway of DMO and DMC formation together with structures of initial states, transition states and final states on Pd_4/TiO_2. Red, silvery, blue, grey and white spheres represent O, Ti, Pd, C and H atoms, respectively.

used as visible-light-driven photocatalysts for selective oxidation of benzyl alcohol [82], but in this work, both Pd_4/TiO_2 and Pd_4/TiO_2-O_v show poor selectivity, it means that the oxygen vacancy on surface has little influence on selectivity of CO oxidative coupling to DMO.

4. Conclusion

In this work, the formation of DMO by CO oxidative coupling were investigated on Pd_4 cluster supported on anatase TiO_2(0 0 1) including perfect and oxygen vacancy surfaces. Pd_4/TiO_2-O_v exhibited higher stability than Pd_4/TiO_2. The *d*-band of two catalysts show that Pd_4/TiO_2-O_v has the weaker adsorption capacity to adsorbates, and the adsorption energy of CO on Pd_4/TiO_2-O_v is weaker than that on Pd_4/TiO_2.

Moreover, the optimal paths on these two catalysts were not changed, Pd_4/TiO_2-O_v showed higher activity towards the reaction by comparing the energy barrier (77.0 *vs.* 146.4 kJ·mol^{-1}) of rate determining steps about two catalysts. Meanwhile, compared with Pd (1 1 1) with the rate determining step energy of 118.4 kJ·mol^{-1}, the Pd_4/TiO_2-O_v still showed higher activity of CO oxidation coupling to

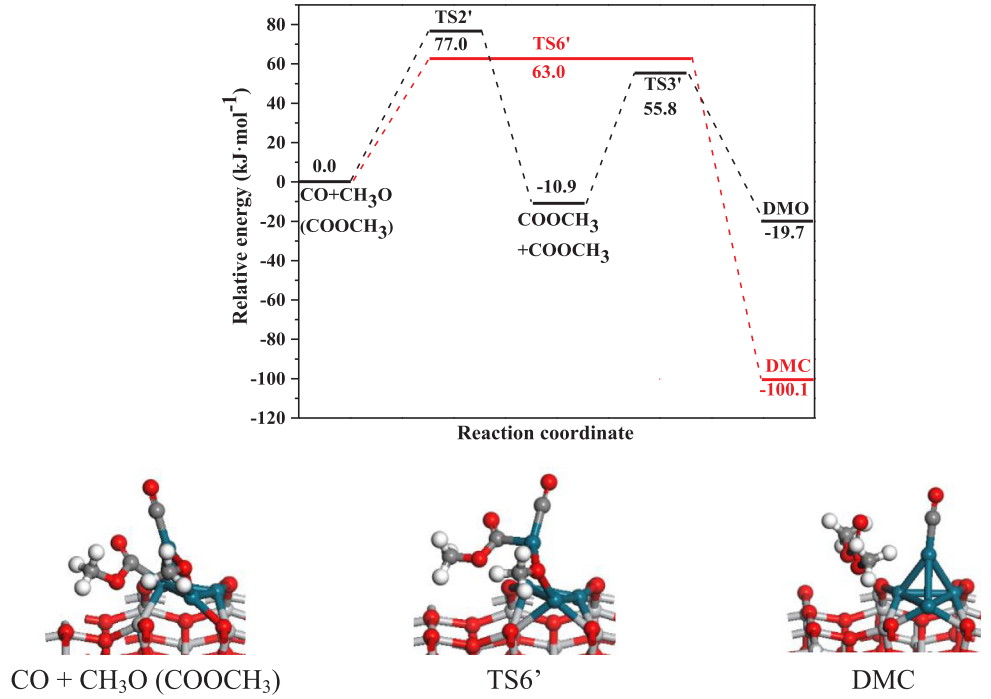

Fig. 11. The comparison of the simplified potential energy profile for the pathway of DMO and DMC formation together with structures of initial states, transition states and final states on Pd_4/TiO_2-O_v. Red, silvery, blue, grey and white spheres represent O, Ti, Pd, C and H atoms, respectively.

DMO. Hence, Pd_4/TiO_2-O_v not only reduce the amount of Pd, but also improved the activity of CO oxidative coupling to DMO. Of course, the selectivity of two catalysts were also considered, however, it was found that poor selectivity of DMO appears on Pd_4/TiO_2 and Pd_4/TiO_2-O_v catalysts.

In addition, the role of oxygen vacancy on support was discussed, the existence of oxygen vacancy enhances the stability of catalyst, and the adsorption capacity of reactants on the catalyst surface was weakened, which makes the adsorbed species easier to migrate on the catalyst and then the catalytic activity was effectively improved, but it had little effect on selectivity.

CRediT authorship contribution statement

Yueting Cao: Conceptualization, Data curation, Formal analysis, Validation, Writing - original draft. **Lixia Ling:** Conceptualization, Data curation, Formal analysis, Funding acquisition, Investigation, Methodology, Project administration, Resources, Software, Validation, Writing - review & editing. **Hao Lin:** Data curation, Writing - original draft. **Maohong Fan:** Writing - review & editing. **Ping Liu:** Writing - review & editing. **Riguang Zhang:** Supervision, Funding acquisition. **Baojun Wang:** Investigation, Methodology, Software, Supervision, Writing - review & editing, Funding acquisition.

Acknowledgments

We gratefully acknowledge financial support from the Key Projects of National Natural Science Foundation of China (No. 21736007), the National Natural Science Foundation of China (Grant Nos. 21576178 and 21476155), Research Project Supported by Shanxi Scholarship Council of China (No. 2016-030) and the Foundation of State Key Laboratory of Coal Conversion (No. J18-19-602).

References

[1] Y. Huang, H. Ariga, X.L. Zheng, X.P. Duan, S. Takakusagi, K. Asakura, Y.Z. Yuan, Silver-modulated SiO_2-supported copper catalysts for selective hydrogenation of dimethyl oxalate to ethylene glycol, J. Catal. 307 (2013) 74–83.
[2] S. Zhao, H. Yue, Y.J. Zhao, B. Wang, Y.C. Geng, J. Lv, S.P. Wang, J.L. Gong, X.B. Ma, Chemoselective synthesis of ethanol via hydrogenation of dimethyl oxalate on Cu/SiO_2: enhanced stability with boron dopant, J. Catal. 297 (2013) 142–150.
[3] Y.F. Zhu, X. Kong, D.B. Cao, J.L. Cui, Y.L. Zhu, Y.W. Li, The rise of calcination temperature enhances the performance of Cu catalysts: contributions of support, ACS Catal. 4 (2014) 3675–3681.
[4] P.P.T. Sah, S.L. Chien, Alkyl oxalates and oxamates, J. Am. Chem. Soc. 53 (1931) 3901–3903.
[5] Y. Yamamoto, Vapor phase carbonylation reactions using methyl nitrite over Pd catalysts, Catal. Surv. Asia 14 (2010) 103–110.
[6] S.Y. Peng, Z.N. Xu, Q.S. Chen, Y.M. Chen, J. Sun, Z.Q. Wang, M.S. Wang, G.C. Guo, An ultra-low Pd loading nanocatalyst with high activity and stability for CO oxidative coupling to dimethyl oxalate, Chem. Commun. 49 (2013) 5718–5720.
[7] M.H. Shao, K. Sasaki, R.R. Adzic, Pd-Fe nanoparticles as electrocatalysts for oxygen reduction, J. Am. Chem. Soc. 128 (2006) 3526–3527.
[8] Y.Z. Lu, W. Chen, Nanoneedle-covered Pd-Ag nanotubes: high electrocatalytic activity for fomic acid oxidation, J. Phys. Chem. C 114 (2010) 21190–21200.
[9] M. Mohl, D. Dobo, A. Kukovecz, Z. Konya, K. Kordas, J.Q. Wei, R. Vajtai, P.M. Ajayan, Formation of CuPd and CuPt bimetallic nanotubes by galvanic replacement reaction, J. Phys. Chem. C 115 (2011) 9403–9409.
[10] G.H. Xu, X.B. Ma, F. He, H.F. Chen, Characteristics of catalyst for carbon monoxide coupling reaction, Ind. Eng. Chem. Res. 34 (1995) 2379–2382.
[11] L.P. Shen, H.Z. Li, L. Lu, Y.F. Luo, Y.W. Tang, Y. Chen, T.H. Lu, Improvement and mechanism of electrocatalytic performance of Pd-Ni/C anodic catalyst in direct formic acid fuel cell, Electrochim. Acta 89 (2013) 497–502.
[12] D. Widmann, Y. Liu, F. Schüth, R.J. Behm, Support effects in the Au-catalyzed CO oxidation - correlation between activity, oxygen storage capacity, and support reducibility, J. Catal. 276 (2010) 292–305.
[13] M. Comotti, W.C. Li, B. Spliethoff, F. Schuth, Support effect in high activity gold catalysts for CO oxidation, J. Am. Chem. Soc. 128 (2006) 917–924.
[14] H. Yoshida, T. Nakajima, Y. Yazawa, T. Hattori, Support effect on methane combustion over palladium catalysts, Appl. Catal. B 71 (2007) 70–79.
[15] P. Sangeetha, K. Shanthi, K.S. RamaRao, B. Viswanathan, P. Selvam, Hydrogenation of nitrobenzene over palladium-supported catalysts—effect of support, Appl. Catal. A 353 (2009) 160–165.
[16] T. Nanba, S. Masukawa, J. Uchisawa, A. Obuchi, Effect of support materials on Ag catalysts used for acrylonitrile decomposition, J. Catal. 259 (2008) 250–259.
[17] R.G. Zhang, M. Peng, B.J. Wang, Catalytic selectivity of Rh/TiO_2 catalyst in syngas conversion to ethanol: probing into the mechanism and functions of TiO_2 support and promoter, Catal. Sci. Technol. 7 (2017) 1073–1085.
[18] X.B. Yu, M.H. Wang, H.X. Li, Study on the nitrobenzene hydrogenation over a Pd-B/SiO_2 amorphous catalyst, Appl. Catal. A: Gen. 202 (2000) 17–22.
[19] Dilip R. Patel, R.N. Ram, Hydrogenation of nitrobenzene using polymer anchored Pd(II) complexes as catalyst, J. Mol. Catal. A: Chem. 130 (1998) 57–64.
[20] Z.Q. Wang, Z.N. Xu, S.Y. Peng, Z.F. Zhuo, P.B. Pan, L. Lin, Y.Y. Qin, G.C. Guo, Y.G. Yao, New catalysts for coal to ethylene glycol, Chinese J. Chem. 35 (2017) 759–768.
[21] X.Z. Jiang, Y.H. Su, B.J. Lee, S.H. Chien, A study on the synthesis of diethyl oxalate over Pd/α-Al_2O_3 catalysts, Appl. Catal. A 211 (2001) 47–51.
[22] T.J. Zhao, D. Chen, Y.C. Dai, W.K. Yuan, A. Holmen, Synthesis of dimethyl oxalate from CO and CH_3ONO on carbon nanofiber supported palladium catalysts, Ind. Eng. Chem. Res. 43 (2004) 4595–4601.
[23] X.G. Zhao, Q. Lin, W.D. Xiao, Characterization of Pd-CeO_2/α-alumina catalyst for synthesis of dimethyl oxalate, Appl. Catal. A 284 (2005) 253–257.
[24] S.Y. Peng, Z.N. Xu, Q.S. Chen, Z.Q. Wang, D.M. Lv, J. Sun, Y. Chen, G.C. Guo, Enhanced stability of Pd/ZnO catalyst for CO oxidative coupling to dimethyl oxalate: effect of Mg^{2+} doping, ACS Catal. 5 (2015) 4410–4417.
[25] Y. Sun, S. Gao, F. Lei, C. Xiao, Y. Xie, Ultrathin two-dimensional inorganic materials: new opportunities for solid state nanochemistry, Acc. Chem. Res. 48 (2014) 3–12.
[26] Y. Zhao, G. Chen, T. Bian, C. Zhou, G.I. Waterhouse, L.Z. Wu, C.H. Tung, L.J. Smith, D. O'Hare, T. Zhang, Defect-rich ultrathin ZnAl-layered doublehydroxide nanosheets for efficient photoreduction of CO_2 to CO with water, Adv. Mater. 27 (2015) 7824–7831.
[27] S. Wang, L. Pan, J.J. Song, W. Mi, J.J. Zou, L. Wang, X. Zhang, Titanium-defected undoped anatase TiO_2 with p-type conductivityroom-temperature ferromagnetism, and remarkable photocatalytic performance, J. Am. Chem. Soc. 137 (2015) 2975–2983.
[28] M.A. Saqlain, A. Hussain, M. Siddiq, A.R. Ferreira, A.A. Leitão, Thermally activated surface oxygen defects at the perimeter of Au/TiO_2: a DFT + U study, Phys. Chem. Chem. Phys. 17 (2015) 25403–25410.
[29] L. Zou, X. Wang, Zhang, Titanium-defected undoped anatase TiO_2 with p-type conductivityroom-temperature ferromagnetism, and remarkable photocatalytic performance, J. Am. Chem. Soc. 137 (2015) 2975–2983.
[30] J. Yang, C.Q. Lv, Y. Guo, G.C. Wang, A DFT + U study of acetylene selective hydrogenation on oxygen defective anatase (101) and rutile (110) TiO2 supported Pd4 cluster, J. Chem. Phys. 36 (2012) 104107.
[31] Y.F. Li, U. Aschauer, J. Chen, A. Selloni, Adsorption and reactions of O_2 on anatase TiO_2, Acc. Chem. Res. 47 (2014) 3361–3368.
[32] N.H. Linh, T.Q. Nguyen, W.A. Diño, H. Kasai, Effect of oxygen vacancy on the adsorption of O_2 on anatase TiO_2(001): a DFT-based study, Surf. Sci. 633 (2015) 38–45.
[33] Y. Han, C.J. Liu, Q.F. Ge, Effect of surface oxygen vacancy on Pt cluster adsorption and growth on the defective anatase TiO_2(101) surface, J. Phys. Chem. C 111 (2007) 16397–16404.
[34] U. Aschauer, Y. He, H. Cheng, S.C. Li, U. Diebold, A. Selloni, Influence of subsurface defects on the surface reactivity of TiO_2: water on anatase (101), J. Phys. Chem. C 114 (2010) 1278–1284.
[35] S. Huygh, E.C. Neyts, Adsorption of C and CH_x radicals on anatase (001) and the influence of oxygen vacancies, J. Phys. Chem. C 119 (2015) 4908–4921.
[36] N.H. Linh, T.Q. Nguyen, W.A. Diño, H. Kasai, Effect of oxygen vacancy on the adsorption of O_2 on anatase TiO_2(001): a DFT-based study, Surf. Sci. 633 (2015) 38–45.
[37] H.Y. Kim, H.M. Lee, G. Henkelman, CO oxidation mechanism on CeO_2-supported Au nanoparticles, J. Am. Chem. Soc. 134 (2012) 1560–1570.
[38] R. Dagani, Nanostructured materials promise to advance range of technologies, Chem. Eng. News 70 (1992) 18–24.
[39] T. Teranishi, M. Miyake, Size control of palladium nanoparticles and their crystal structures, Chem. Mater. 10 (1998) 594–600.
[40] Y.X. Pan, C.J. Liu, Q.F. Ge, Effect of surface hydroxyls on selective CO_2 hydrogenation over Ni_4/γ-Al_2O_3: A density functional theory study, J. Catal. 272 (2010) 227–234.
[41] J.W.deM. Carneiro, M.T.deM. Cruz, Density functional theory study of the adsorption of formaldehyde on Pd_4 and on Pd_4/γ-Al_2O_3 clusters, J. Phys. Chem. A 112 (2008) 8929–8937.
[42] A.G. Zacarias, M. Castro, J.M. Tour, J.M. Seminario, Lowest energy states of small Pd clusters using density functional theory and standard ab Initio methods. A route to understanding metallic nanoprobes, J. Phys. Chem. A 103 (1999) 7692–7700.
[43] C.H. Sun, S.C. Smith, Strong interaction between gold and anatase TiO_2(001) predicted by first Principle studies, J. Phys. Chem. C 116 (2012) 3524–3531.
[44] G. Kresse, J. Furthmüller, Efficiency of ab-initio total energy calculations for metals and semiconductors using a plane-wave basis set, Comput. Mater. Sci. 6 (1996) 15–50.
[45] G. Kresse, J. Hafner, Ab initio molecular dynamics for open-shell transition metals, Phys. Rev. B 48 (1993) 13115–13118.
[46] G. Kresse, J. Furthmüller, Efficient iterative schemes for ab initio total-energy calculations using a plane-wave basis set, Phys. Rev. B 54 (1996) 11169–11186.
[47] G. Kresse, D. Joubert, From ultrasoft pseudopotentials to the projector augmented-wave method, Phys. Rev. B 59 (1999) 1758–1775.
[48] J.P. Perdew, K. Burke, M. Ernzerhof, Generalized gradient approximation made simple, Phys. Rev. Lett. 77 (1996) 3865–3868.
[49] W.G. Chen, P.F. Yuan, S. Zhang, Q. Sun, E. Liang, Y. Jia, Electronic properties of anatase TiO_2, doped by lanthanides: a DFT + U study, Phys. B Condens. Matter 407

(2012) 1038–1043.
[50] M.M. Islam, M. Calatayud, Pacchioni G. Hydrogen, Adsorption and diffusion on the anatase TiO_2(101) surface: a first-principles investigation, J. Phys. Chem. C 115 (2011) 6809–6814.
[51] G. Han, S. Hu, S. Yan, L. Mei, Oxygen vacancy induced ferromagnetism in rutile TiO_{2-x}, Phys. Status Solidi 3 (2009) 148–150.
[52] E. Finazzi, C.D. Valentin, G. Pacchioni, A. Selloni, Excess electron states in reduced bulk anatase TiO_2: comparison of standard GGA, GGA + UGGA + U, and hybrid DFT calculations, J. Chem. Phys. 129 (2008) 154113.
[53] L. Fernández-Werner, R. Faccio, A. Juan, A. Juan, H. Pardo, B. Montenegro, Á.W. Mombrú, Ultrathin (001) and (100) TiO_2(B) sheets: surface reactivity and structural properties, Appl. Sur. Sci. 290 (2014) 180–187.
[54] G. Henkelman, B.P. Uberuaga, H. Jónsson, A climbing image nudged elastic band method for finding saddle points and minimum energy paths, J. Chem. Phys. 113 (2000) 9901–9904.
[55] G. Henkelman, H. Jónsson, Improved tangent estimate in the nudged elastic band method for finding minimum energy paths and saddle points, J. Chem. Phys. 113 (2000) 9978–9985.
[56] G. Henkelman, H. Jónsson, A dimer method for finding saddle points on high dimensional potential surfaces using only first derivatives, J. Chem. Phys. 111 (1999) 7010–7022.
[57] R.A. Olsen, G.J. Kroes, G. Henkelman, A. Arnaldsson, H. Jónsson, Comparison of methods for finding saddle points without knowledge of the final states, J. Phys. Chem. 121 (2004) 9776–9792.
[58] J.K. Burdett, T. Hughbanks, G.J. Miller, J.W. Richardson, J.V. Smith, Structural-electronic relationships in inorganic solids: powder neutron diffraction studies of the rutile and anatase polymorphs of titanium dioxide at 15 and 295 K, J. Am. Chem. Soc. 109 (1987) 3639–3646.
[59] M.A. Saqlain, A. Hussain, M. Siddiq, A.R. Ferreira, A.A. Leitão Phys, Thermally activated surface oxygen defects at the perimeter of Au/TiO_2: a DFT + U study, Phys. Chem. Chem. Phys. 17 (2015) 25403–25410.
[60] Y. Ortegaa, D.F. Heviaa, J. Oviedo, M.A. San-Miguel, A DFT study of the stoichiometric and reduced anatase (001) surfaces, Appl. Surf. Sci. 294 (2014) 42–48.
[61] X. Wang, Z. Rui, Y. Zeng, H. Ji, Z. Du, Q. Rao, Synergetic effect of oxygen vacancy and Pd site on the interaction between Pd/anatase TiO_2(101) and formaldehyde: a density functional theory study, Catal. Today 297 (2017) 151–158.
[62] D. Jiang, S. Dai, The role of low-coordinate oxygen on Co_3O_4(110) in catalytic CO oxidation, Phys. Chem. Chem. Phys. 13 (2010) 978–984.
[63] P. Deák, J. Kullgren, T. Frauenheim, Polarons and oxygen vacancies at the surface of anatase TiO_2, Phys. Status Solidi RRL 6 (2014) 583–586.
[64] T. Bredow, G. Pacchioni, Electronic structure of an isolated oxygen vacancy at the TiO_2(110) surface, Chem. Phys. Lett. 355 (2002) 417–423.
[65] M. Nolan, S.C. Parker, G.W. Watson, The electronic structure of oxygen vacancy defects at the low index surfaces of ceria, Surf. Sci. 595 (2005) 223–232.
[66] J.L. Zhang, M. Zhang, Y. Han, W. Li, X.K. Meng, B.N. Zong, Nucleation and growth of palladium clusters on anatase TiO_2(101) surface: a first principle study, J. Phys. Chem. C 112 (2008) 19506–19515.
[67] Y. Wang, E. Florez, F. Mondragon, T.N. Truong, Effects of metal–support interactions on the electronic structures of metal atoms adsorbed on the perfect and defective MgO(100) surfaces, Surf. Sci. 600 (2006) 1703–1713.
[68] N. Acerbi, S.C.E. Tsang, G. Jones, S. Golunski, P. Collier, Rationalization of interactions in precious metal/ceria catalysts using the *d*-band center model, Angew. Chem. Int. Ed. 52 (2013) 7737–7741.
[69] S.D. Miller, J.R. Kitchin, Relating the coverage dependence of oxygen adsorption on Au and Pt fcc(111) surfaces through adsorbate-induced surface electronic structure effects, Surf. Sci. 603 (2009) 794–801.
[70] J.D. Li, E. Croiset, L. Ricardez-Sandoval, Methane dissociation on Ni (100), Ni (111), and Ni (553): a comparative density functional theory study, J. Mol. Catal. A: Chem. 365 (2012) 103–114.
[71] Y. Liu, Q. Wang, H.Y. Liu, K. Li, D.B. Li, B. Hou, B.J. Wang, Insights into the metal-support interaction between NiCu cluster and MgO as well as its effect on H adsorption and H_2 dissociation, Mol. Catal. 436 (2017) 111–119.
[72] L.A. Kibler, A.M. El-Aziz, R. Hoyer, D.M. Kolb, Tuning reaction rates by lateral strain in a palladium monolayer, Angew. Chem. Int. Ed. 44 (2005) 2080–2084.
[73] C. Fan, M. Luo, W.D. Xiao, Reaction mechanism of methyl nitrite dissociation during co catalytic coupling to dimethyl oxalate: a density functional theory study, Chinese J. Chem. Eng. 24 (2016) 132–139.
[74] B.Y. Han, X. Feng, L.X. Ling, M.H. Fan, Ping Liu, R.G. Zhanga, B.J. Wang, CO oxidative coupling to dimethyl oxalate over Pd–Me (Me = Cu, Al) catalysts: a combined DFT and kinetic study, Phys. Chem. Chem. Phys. 20 (2018) 7317–7332.
[75] X. Feng, L.X. Ling, Y.T. Cao, R.G. Zhang, M.H. Fan, B.J. Wang, A DFT study on the catalytic CO oxidative coupling to dimethyl oxalate on Al-doped core − shell Pd clusters, J. Phys. Chem. C 122 (2018) 1169–1179.
[76] L.X. Ling, X. Feng, Y.T. Cao, P. Liu, M.H. Fan, R.G. Zhang, B.J. Wang, The catalytic CO oxidative coupling to dimethyl oxalate on Pd clusters anchored on defected graphene: a theoretical study, Mol. Catal. 453 (2018) 100–112.
[77] Q.H. Li, Z.F. Zhou, R.P. Chen, B.Z. Sun, L.Y. Qiao, Y.G. Yao, K.C. Wu, Insights into the reaction mechanism of CO oxidative coupling to dimethyl oxalate over palladium: a combined DFT and IR study, Phys. Chem. Chem. Phys. 17 (2015) 9126–9134.
[78] S.Y. Peng, Z.N. Xu, Q.S. Chen, Z.Q. Wang, Y. Chen, D.M. Lv, G. Lu, G.C. Guo, MgO: an excellent catalyst support for CO oxidative coupling to dimethyl oxalate, Catal. Sci. Technol. 4 (2014) 1925–1930.
[79] Z.N. Xu, J. Sun, C.S. Lin, X.M. Jiang, Q.S. Chen, S.Y. Peng, M.S. Wang, G.C. Guo, High-performance and long-lived Pd nanocatalyst directed by shape effect for CO oxidative coupling to dimethyl oxalate, ACS Catal. 3 (2013) 118–122.
[80] H.Y. Liu, B.T. Teng, M.H. Fan, B.J. Wang, Y.L. Zhang, H.G. Harris, CH_4 dissociation on the perfect and defective MgO(001) supported Ni_4, Fuel 123 (2014) 285–292.
[81] G. Pacchioni, L. Giordano, A.M. Ferrari, S. Abbet, U. Heiz, Role of point defects in the catalytic activation of Pd atoms supported on the MgO Surface, Theoret. Aspects Heterogen. Catal. 8 (2001) 183–198.
[82] X.Y. Pan, Y.J. Xu, Defect-mediated growth of noble-metal (Ag, Pt, and Pd) nanoparticles on TiO_2 with oxygen vacancies for photocatalytic redox reactions under visible light, J. Phys. Chem. C 117 (2013) 17996–18005.